

Advanced KF-based Methods for GNSS Carrier Tracking and Ionospheric Scintillation Mitigation

Jordi Vilà-Valls, Pau Closas and Carles Fernández-Prades
Centre Tecnològic de Telecomunicacions de Catalunya (CTTC), 08860, Barcelona, Spain
Email: {jvila, pclosas, cfernandez}@cttc.cat

Abstract—Ionospheric scintillation is the name given to the disturbance caused by electron density irregularities along the propagation path of electromagnetic waves through the ionosphere. These non-nominal propagation conditions mainly cause carrier phase variations and amplitude fades. It is important to point out that both degradations are correlated, and thus deep amplitude fades and rapid phase variations (the so-called canonical fades) occur in a simultaneous and random manner. Regarding the carrier synchronization problem under harsh propagation conditions, such as high dynamics, multipath effects or ionospheric scintillation, canonical fades make the latter the most challenging scenario, which can be considered as a benchmark on the performance of robust carrier tracking techniques. This phenomenon particularly affects satellite-based positioning systems in the equatorial regions and at high latitudes. In this work, both amplitude and phase variations due to scintillation are first modeled using an autoregressive (AR) model, and then included into the system state-space formulation. Therefore, a Kalman filter (KF) based solution can be aware of both dynamics and scintillation phase evolutions. This arises as the natural solution to mitigate those undesired propagation effects. Moreover, in order to counteract the main drawbacks of standard KF-based tracking solutions, an extended KF (EKF) architecture is considered, tracking both the phase dynamics, scintillation phase and amplitude. This implies directly operating with the baseband received signal's complex samples, avoiding the use of discriminators and thus its saturation and the loss of Gaussianity. Simulation results are provided to support the theoretical discussion and to show the performance improvements of such new approach.

TABLE OF CONTENTS

1	INTRODUCTION	1
2	IONOSPHERIC SCINTILLATION	2
3	SIGNAL MODEL	4
4	ON STANDARD GNSS CARRIER TRACKING	6
5	JOINT CARRIER TRACKING AND SCINTILLATION MITIGATION	7
6	COMPUTER SIMULATIONS	8
7	CONCLUSIONS	9
	REFERENCES	9
	BIOGRAPHY	10

1. INTRODUCTION

Synchronization is a key stage in any communication receiver or positioning system, and is typically carried out following a two-state approach: acquisition and tracking. The first stage

provides a coarse estimate of the synchronization parameters (i.e., timing and frequency), and the second one refines those estimates, filtering out noise and tracking any possible time-variation [1]. The problem under study concerns the derivation of efficient and robust methods for carrier phase tracking and ionospheric scintillation mitigation in Global Navigation Satellite Systems (GNSS). Mass-market GNSS receivers typically implement traditional carrier tracking techniques based on well-established phase-locked loop (PLL) architectures [2], which are only reliable for quite benign propagation conditions, and thus they are not suitable to cope with moderate to severe scintillation conditions. In the last decade, the Kalman filter (KF) based solutions have been shown to be flexible, robust and the method of choice to overcome the limitations of standard architectures, but in their standard form do not provide a solution to the scintillation mitigation problem.

General Considerations

The following assumptions have been undertaken along this paper:

- Acquisition is not considered and a perfect time-delay synchronization is assumed.
- Among the possible non-nominal propagation conditions (e.g., high dynamics, shadowing, strong fading, multipath effects or ionospheric scintillation) only the ionospheric scintillation is considered. Because of the so-called canonical fades [3], these are certainly the most challenging propagation conditions in terms of carrier phase tracking, and in general can be considered as a tracking performance benchmark.
- The fact that scintillation effects are typically unnoticed for mass-market GNSS receivers has led this effect to receive rather little attention in the signal processing literature, that is why few contributions appear in the literature and advanced signal processing techniques have not been applied yet to the scintillation mitigation problem.
- Both PLL-based approaches and standard KF-based solutions are considered as the state-of-the-art carrier tracking baseline architectures.

Carrier Tracking State-of-the-Art

The problem of standard PLLs is the well-known noise reduction/dynamic range trade-off (i.e., a small bandwidth is needed to be able to filter out the noise and track signals with low carrier to noise ratios (C/N_0), and a large bandwidth has to be used to cope with high dynamics), which is mainly driven by the bandwidth and order of the loop. These techniques have been shown to deliver poor estimates or even fail under harsh propagation conditions [4, 5]. On the basis of conventional PLL architectures, some improvements have been proposed in the literature: hybrid architectures coupling the PLL with a frequency-locked loop (FLL) to reduce the dynamics of the signal to be tracked [6], wavelet denoising techniques to reduce the noise affecting the system [4], or adaptive methods that sequentially adapt the bandwidth of

This work has been partially supported by the European Commission in the Network of Excellence in Wireless COMMunications NEWCOM# (contract n. 318306), the Spanish Ministry of Economy and Competitiveness project TEC2012-39143 (SOSRAD), and by the Government of Catalonia (2014-SGR-1567).

the system according to the actual working conditions [7, 8]. A good and up-to-date survey on robust carrier tracking techniques is given by [9].

The performance of all these PLL-based techniques have been clearly overcome by Kalman filter (KF)-based tracking techniques [5, 10–13], which are formulated from an optimal filtering approach and where the filter is automatically adjusted so as to minimize the mean square error. That is why these methods are in the core of the most advanced carrier phase tracking techniques. But not everything is nice in the standard KF approach: the main drawback is the need of an exact knowledge of the process and measurement noise statistics for an optimal and correct behavior, therefore being constrained by the accuracy of the dynamic model and the a priori fixed system parameters. In practical real-life applications, these quantities need to be estimated or somehow adjusted to provide a robust solution. Some strategies appear in the literature to overcome those limitations. The so-called Adaptive KFs (AKFs) try to sequentially adapt the filter parameters (e.g., the process and measurement noise covariance matrices) to the actual working conditions, usually using an heuristic/ad-hoc approach [14, 15], innovations-based solutions for one of the two parameters of interest [14, 16] or the C/N_0 estimates to easily adjust the measurement noise statistics [17]. But a general framework for the correct design of adaptive KFs dealing with both process and measurement noises does not exist, and it is an important missing point in the carrier tracking literature (see [18] for a tentative answer and a comprehensive discussion on this subject).

Taking into account the problem at hand, that is, the ionospheric scintillation mitigation, the main problem of both existing PLL and KF-based approaches is the *estimation versus mitigation dilemma*: if the carrier synchronization technique is well designed to correctly track the input signal dynamics, it will also track the phase variations due to the scintillation effect, then being impossible to separate both contributions and mitigate this undesired effect. In other words, a standard receiver should implement a PLL or KF being able to track (slowly) time-varying Doppler shifts (e.g., Doppler frequency drift and Doppler frequency rate), therefore being capable to track or lock to rapidly varying phase changes. Under this situation, when the carrier phase is corrupted by ionospheric scintillation the receiver interprets the fast phase changes as fast frequency shifts and consequently tries to track the complete phase (i.e., only filtering out noise). How to solve this problem? The filter itself must be able to separate both contributions. One of the major advantages of the KF is its flexible state-space formulation, which makes possible a state augmentation to include any prior information on the system or propagation conditions. Therefore, if the scintillation process is somehow modeled so as to be embedded into the filter formulation, the filter would be aware of both contributions and an effective scintillation mitigation could be envisaged. This arises as the natural solution to mitigate those undesired propagation effects.

Contribution

The idea of modeling the scintillation process and including it into the state-space formulation is not completely new. Modeling the ionospheric scintillation phase as an autoregressive $AR(1)$ process was first introduced in [19], where it was embedded into an Interacting Multiple Model (IMM) to deal with time-varying conditions, and then tested with real scintillation signal in a static scenario in [20], but both analysis where in a very preliminary stage. In this work, not only the phase is modeled as an AR process but also the amplitude of

the complex scintillation process. Then, a state-space model is build to take into account both scintillation components. Using this augmented state-space formulation the filter is aware of both dynamics and scintillation phase evolution together with the scintillation amplitude fades. Moreover, to counteract the main drawbacks of standard KF-based tracking solutions, which adopt the traditional PLL architecture based on a discriminator plus filter structure, an extended KF (EKF) approach is considered. This modified architecture directly operates with the baseband received signal complex samples and tracks the phase dynamics, scintillation phase and amplitude. Using this improved architecture (i.e., with respect of what was done in [19] and [20]), the possible discriminator saturation and loss of Gaussianity (what implies a suboptimal KF operation) are avoided.

The paper is organized as follows: Section 2 introduces the ionospheric scintillation and its approximation using and AR process. The GNSS carrier signal model and state-space formulation are given in Section 3. Section 4 briefly summarizes the standard state-of-the-art carrier tracking techniques and the new solution is introduced in Section 5. Simulation results are provided in Section 6 to support the theoretical discussion and to show the performance improvements of such new approach.

2. IONOSPHERIC SCINTILLATION

Ionospheric scintillation is the name given to the disturbance caused by electron density irregularities along the propagation path through the ionosphere. These irregularities affect every earth-to-space communication link, and the signal degradations mainly depend on the frequency band, the ray path angle, the solar activity and the Earth region. In particular, these non-nominal propagation conditions corrupt GNSS signals with amplitude fades and carrier phase variations, which may lead to navigation bit errors, carrier phase cycle slips or complete loss of lock. It is important to notice that these amplitude fades and phase changes happen in a simultaneous and random manner, but there exists a correlation between both disturbances, the so-called canonical fades. That is, the largest amplitude fades are usually associated with half-cycle phase jumps [3], which is a very challenging scenario from a carrier tracking point of view. Two main reasons have led ionospheric scintillation to receive little attention in the signal processing literature: first, ionospheric scintillation particularly affects GNSS receivers in equatorial regions (in the post-sunset to midnight local-time sector) and at high latitudes (within and poleward of the auroral region), and therefore its effects are typically unnoticed for the vast majority of mass-market GNSS receivers, whose dominant degradations are caused by thermal noise and multipath reflections. For instance, most of the existing contributions related to scintillation are focused on very specific scientific-related topics and are often of limited suitability in GNSS signal processing applications.

Scintillation model

A lot of effort has been put the past decade to characterize the ionospheric scintillation, mainly to obtain effective synthetic models to assess GNSS receivers' performance via simulation. This is particularly useful to obtain statistically significant performance results, which cannot be obtained using real scintillation data. There exist three different ways to obtain such synthetic data [21]: physics-based models, phase screen models and statistical models. From the different alternatives available in the literature, the most relevant

are the Cornell Scintillation Model (CSM) [21, 22] and the Global Ionospheric Scintillation Model (GISM) [23]. The latter is based on a phase screen technique driven by the NeQuick electron density climatological model [24], while the former is based on a statistical model and the proper shaping of the spectrum of the entire complex scintillation signal. Even if the recommendation from the International Telecommunication Union (ITU) is to use the GISM for the design of satellite services and systems, the CSM is much more convenient from a simulation point of view and is the one being used throughout this paper.

The purpose of this section is to introduce a parsimonious signal model to represent the behavior of scintillation onto the GNSS received signal samples. In terms of the complex-valued baseband received signal, $x(t)$, the scintillation can be modeled as a multiplicative channel,

$$x(t) = \xi_s(t)s(t) + w(t), \quad (1)$$

where, $s(t)$ is the complex-valued baseband equivalent of the transmitted signal, $w(t)$ is the noise term, which may include the thermal noise, replicas of the transmitted signal due to multipath, and any other interference, and the complex-valued stochastic process representing the presence of scintillation is defined as,

$$\xi_s(t) = \rho_s(t)e^{j\theta_s(t)}, \quad (2)$$

with the corresponding envelope and phase components, $\rho_s(t)$ and $\theta_s(t)$. Because of the interdependence between both magnitudes (i.e., amplitude and phase) which is apparent in the presence of canonical fades [25], the characterization of their individual distributions, widely used in the scintillation modeling literature, is not a valid approach.

The strength of amplitude scintillation is described by the so-called scintillation index S_4 , and is usually considered within three main regions [21]: weak, moderate and strong/severe scintillation, and is defined as

$$S_4 = \sqrt{\frac{\mathbb{E}(\rho_s^4) - (\mathbb{E}(\rho_s^2))^2}{(\mathbb{E}(\rho_s^2))^2}} \quad \begin{cases} S_4 \leq 0.3 & (weak) \\ 0.3 < S_4 \leq 0.6 & (mod.) \\ 0.6 < S_4 & (sev.) \end{cases}$$

The envelope of this amplitude scintillation is typically modeled as a Nakagami-m random variable (r.v.), but the experimental results in [21] show that a simpler Ricean distribution can also be used, while preserving a close fit with empirical data. This is a very convenient approach for simulation purposes, because it means that the complex-valued scintillation $\xi_s(t)$ can easily be modeled as a complex Gaussian r.v. with a given autocorrelation $R_{\xi_s}(\tau)$,

$$\rho_s \sim \text{Ricean}(K_{\rho_s}, \Omega_{\rho_s}) \rightarrow \xi_s \sim \mathcal{CN}(\mu_{\rho_s}, \sigma_{\rho_s}^2), \quad (3)$$

with the following parameters: $K_{\rho_s} = \frac{\mu_{\rho_s}^2}{2\sigma_{\rho_s}^2}$, $\Omega_{\rho_s} = \mu_{\rho_s}^2 + \sigma_{\rho_s}^2$, $\mu_{\rho_s} = \mathbb{E}(\rho_s)$ and $\sigma_{\rho_s}^2 = \mathbb{E}(\rho_s^2) - (\mathbb{E}(\rho_s))^2$.

Notice that for the simulation of a scintillation data set only two parameters must be specified, $\{S_4, \tau_0\}$, which determine the intensity and correlation of the scintillation complex gain components, respectively. In general, higher S_4 and lower τ_0 lead to more severe scintillation, where the ranges of possible values are $0 < S_4 \leq 1$ and $0.1 \leq \tau_0 < 2$ seconds, respectively [21]. The

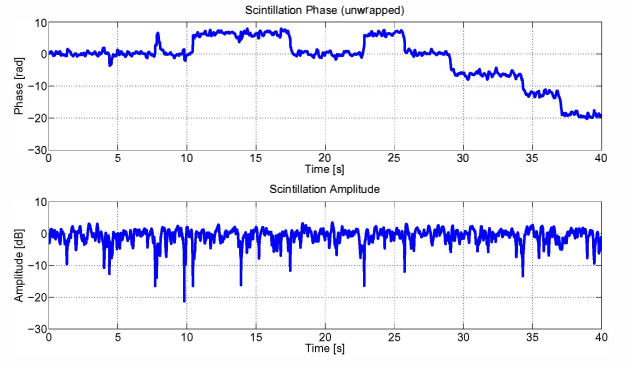


Figure 1. Severe scintillation CSM time-series example. Unwrapped scintillation phase in radians (top) and scintillation amplitude (bottom).

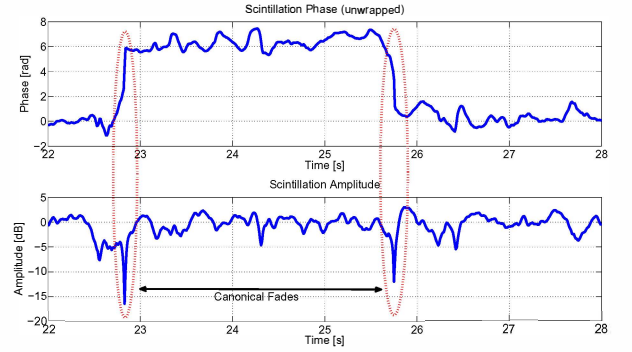


Figure 2. Severe scintillation CSM time-series example. Zoom of Figure 1 to clearly show the existence of canonical fades. Phase in radians.

CSM has been embedded in the so-called Cornell Scintillation Simulation Matlab toolkit, which is available at <http://gps.ece.cornell.edu/tools.php>.²

An example of a severe scintillation time-series generated with the CSM is shown in Figure 1. The synthetic data (40 seconds) was generated with $S_4 = 0.8$, $\tau_0 = 0.1$, and sampled at $f_s = 100$ Hz. Notice that in the scintillation amplitude plot there are fades as low as -20 dB, and it is easy to see in the unwrapped scintillation phase several jumps. A zoom is shown in Figure 2 to clearly identify the canonical fades appearing in such severe scintillation scenario, where the phase jumps are associated with deep amplitude fades.

Scintillation approximation

The scintillation models and simulators available in the literature are very useful to synthesize realistic scintillation time-series. The main goal of this contribution is to propose new techniques for scintillation mitigation, with the aim to overcome the limitations of current state-of-the-art GNSS tracking approaches, thus the capability to test realistic scenarios is fundamental. But apart from the simulation point of view, which is covered with realistic models, it may be interesting to have a simple mathematical model approximation to be exploited in the receiver side. How to use and take advantage of the approximation presented in this section is discussed in

²This software will be used in the computer simulations to generate the desired scintillation effect and then assess the performance of the proposed methods.

the following sections.

The shape of the empirical phase and amplitude spectra given in [21] and [23], and the fact that the CSM simulates the scintillation complex gain using a second-order low-pass Butterworth filter, let us assume that the correlation in both components can be fairly well modeled using an autoregressive (AR) process. For severe scintillation, which is the most challenging scenario for current state-of-the-art carrier phase tracking techniques, the scintillation phase can be modeled using an $AR(1)$ process and the scintillation amplitude considering an $AR(2)$ process.

The general $AR(1)$ model for a discrete sequence z_k is specified by the following recursion,

$$z_k = \beta_{1,1}z_{k-1} + \eta_k, \quad (4)$$

where η_k is a white Gaussian noise sequence with variance σ_η^2 . The coefficient $\beta_{1,1}$ and the variance σ_η^2 can be obtained through the Yule-Walker equations [26], using the autocorrelation function of the sequence z_k , which is denoted, for an autocorrelation lag m , $R_{zz}(m)$. For an $AR(1)$ process, the required parameters can easily be obtained as,

$$\beta_{1,1} = \frac{R_{zz}(1)}{R_{zz}(0)} ; \quad \sigma_\eta^2 = R_{zz}(0) - \beta_{1,1}R_{zz}(1). \quad (5)$$

Considering the same discrete sequence z_k , the $AR(2)$ process model recursion is written as

$$z_k = \beta_{2,1}z_{k-1} + \beta_{2,2}z_{k-2} + \eta_k, \quad (6)$$

and the corresponding parameters are obtained as

$$\begin{bmatrix} \beta_{2,1} \\ \beta_{2,2} \end{bmatrix} = \begin{bmatrix} R_{zz}(0) & R_{zz}(1) \\ R_{zz}(1) & R_{zz}(0) \end{bmatrix}^{-1} \begin{bmatrix} R_{zz}(1) \\ R_{zz}(2) \end{bmatrix}, \quad (7)$$

and

$$\sigma_\eta^2 = R_{zz}(0) - \beta_{2,1}R_{zz}(1) - \beta_{2,2}R_{zz}(2). \quad (8)$$

Notice that the scintillation amplitude process has a mean around 1 and the $AR(2)$ process in (6) is zero mean by definition. Therefore, to fit an $AR(2)$ model to the scintillation amplitude the formulation must be generalized as

$$z_k = c + \beta_{2,1}z_{k-1} + \beta_{2,2}z_{k-2} + \eta_k, \quad (9)$$

with c a constant value, and the mean of the process equal to $\mu = c/(1 - \beta_{2,1} - \beta_{2,2})$.

The scintillation time histories generated with the CSM can be used to fit the $AR(1)$ or $AR(2)$ models to the synthetic scintillation phase and amplitude, and thus, to obtain the corresponding parameters using the autocorrelation functions of such time-series. For the $AR(2)$ case, the model fitting has been done using Matlab's `arima` function to take into account the constant value c . To give an example and reusing the time-series plotted in Figure 1 ($S_4 = 0.8$, $\tau_0 = 0.1$, $f_s = 100$ Hz), the following parameters were obtained:

$$\begin{cases} \text{Amplitude} & \rightarrow \begin{cases} \beta_{2,1} = 1.794 \\ \beta_{2,2} = -0.827 \\ \sigma_{\eta_a}^2 = 0.0018 \\ c = 0.03 \end{cases} \\ \text{Phase} & \rightarrow \begin{cases} \beta_{1,1} = 0.915 \\ \sigma_{\eta_\phi}^2 = 0.082 \end{cases} \end{cases}.$$

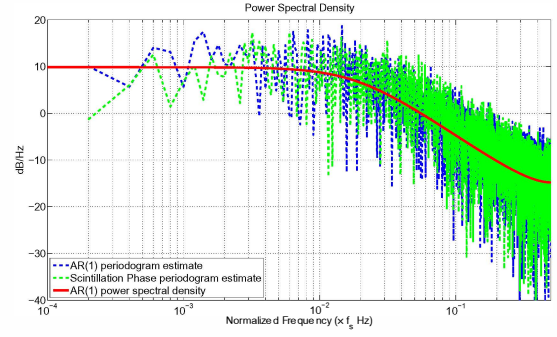


Figure 3. Severe scintillation CSM time-series example. Scintillation phase empirical spectrum and fitted $AR(1)$ process.

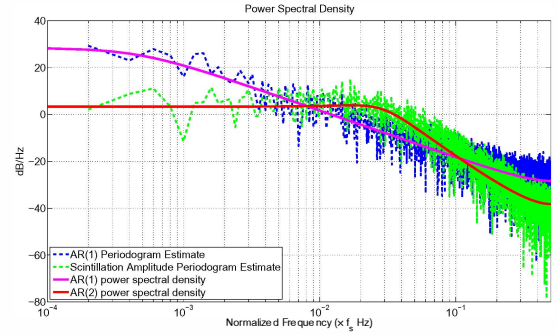


Figure 4. Severe scintillation CSM time-series example. Scintillation amplitude empirical spectrum and fitted $AR(2)$ process.

To close the loop and discussion on the AR modeling of the ionospheric scintillation, and again considering the previous example, the empirical and fitted AR process power spectral densities (psd) are shown for both phase and amplitude in Figures 3 and 4, respectively. To summarize:

- Figure 3: the empirical scintillation phase psd (dashed green), obtained from the scintillation CSM time-series, is plotted together with the $AR(1)$ process psd (solid red) and the empirical psd of an $AR(1)$ time-series (dashed blue) generated with the same parameters. Both the empirical and the theoretical frequency response correctly fit the empirical scintillation.
- Figure 4: the empirical scintillation amplitude psd (dashed green) is plotted together with the $AR(2)$ process psd (solid red). The psd of an $AR(1)$ time-series (dashed blue) generated with the $AR(1)$ parameters fitted to the scintillation amplitude, together with the psd of an $AR(1)$ with the same parameters (solid magenta), are plotted to support the need of the $AR(2)$ model for the scintillation amplitude.

From these figures, it is clear that both AR processes are convenient for the desired phase and amplitude modeling.

3. SIGNAL MODEL

GNSS signal model

The baseband analytic representation of a generic GNSS transmitted signal can be expressed as

$$s(t) = P_x(t)d(t - \tau(t))c(t - \tau(t))e^{j\theta(t)}, \quad (10)$$

where $P_x(t)$, $d(t)$ and $c(t)$, stand for the signal amplitude, the navigation message and the spreading code, respectively. The synchronization parameters are the code delay, $\tau(t)$, and the carrier phase, $\theta(t)$. The latter can be formulated as $\theta(t) = 2\pi f_d(t) + \theta_e(t)$, where $f_d(t)$ is the carrier Doppler frequency shift and $\theta_e(t)$ a carrier phase component including the other phase impairments. The digitized signal (sampling period T_s) at the output of the radio frequency (RF) front-end feeds the digital receiver M channels. The goal of each channel is to acquire and track the signal of a single satellite. After the acquisition stage, which provides the first code delay and Doppler shift estimates, respectively, $\hat{\tau}(t)$ and \hat{f}_d , the sampled signal is correlated with a locally-generated replica and then accumulated over the integration period T_s . The samples at the output of the correlators are [27]:

$$y_k = A_k d_k R(\Delta\tau_k) \frac{\sin(\pi \Delta f_{d,k} T_s)}{\pi \Delta f_{d,k} T_s} e^{j(2\pi \Delta f_{d,k} T_s + \Delta\theta_k)} + n_k, \quad (11)$$

where k stands for the discrete time $t_k = kT_s$, A_k is the signal amplitude at the output of the correlators after accumulation over T_s , d_k is the data bit, $R(\cdot)$ is the code correlation function and $\{\Delta\tau_k, \Delta f_{d,k}, \Delta\theta_k\}$ are, respectively, the code delay, Doppler shift and carrier phase errors. The noise at the output of the correlators is considered additive Gaussian with variance $\sigma_{n,k}^2$, that is, $n_k \sim \mathcal{N}(0, \sigma_{n,k}^2)$.

Taking into account the problem at hand (*i.e.*, study of new advanced carrier phase estimation techniques for scintillation mitigation), a simplified signal model with a perfect code delay estimation, $\Delta\tau_k = 0$, can be considered. Moreover, it is also considered that $R(0) = 1$, no data bits are present in the received samples (*i.e.*, this is the case when using pilot signals or data wipe-off techniques), and that the attenuation factor is negligible, $\text{sinc}(\Delta f_{d,k} T_s) \approx 1$. Under these assumptions, the simplified model for the samples at the input of the carrier phase tracking stage is

$$y_k = \alpha_k e^{j\theta_k} + n_k, \quad (12)$$

where the amplitude, α_k , may include the scintillation amplitude effects, $\alpha_k = A_k \rho_{s,k}$; and the carrier phase includes both the phase variations due to the receiver's dynamics, $\theta_{d,k}$, and the scintillation phase variation, $\theta_{s,k}$, resulting in $\theta_k = \theta_{d,k} + \theta_{s,k}$.

Impact of scintillation into the carrier phase

In perfect clear sky propagation conditions, the carrier phase in the samples given by (12) should only be affected by the relative motion between the satellite and the receiver (*i.e.*, $\theta_k = \theta_{d,k}$ and $\alpha_k = A_k$). In general, real-life propagation conditions and hardware imperfections include several impairments, namely, phase distortion due to multipath propagation, non-line-of-sight, receiver phase noise or ionospheric scintillation. The latter directly affects the received signal carrier phase with a small distortion in benign scintillation conditions, but with phase jumps and highly varying phase transitions under severe conditions, what turns to be very challenging from a carrier tracking perspective.

An example is given in Figure 5, where the severe scintillation of the previous examples was considered ($S4 = 0.8$, $\tau_0 = 0.1$ s, $f_s = 100$ Hz), and the initial Doppler shift was set to 2 Hz and the Doppler rate to 0.01 Hz/s. The effect of the canonical fades is evident in the unwrapped phase (bottom plot). The main tracking challenge is to avoid these phase jumps and somehow mitigate such undesired effect, what

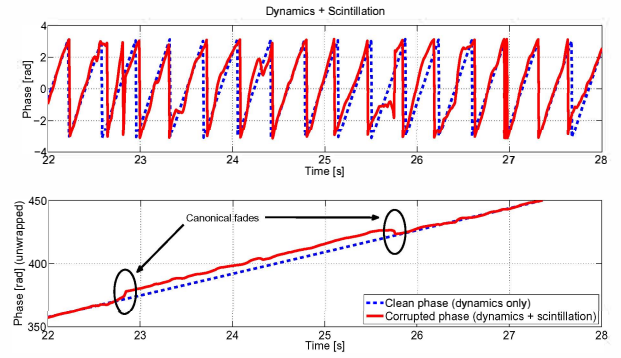


Figure 5. Effect of severe ionospheric scintillation into the carrier phase. Top - wrapped phase. Bottom - unwrapped phase.

is actually impossible with current state-of-the-art receivers because of the existing estimation versus mitigation trade-off previously discussed.

State-space formulation

In the carrier phase tracking problem, considering that the input to the tracking block is given by (12), the parameter of interest is the phase θ_k . This phase is usually modeled using a Taylor approximation of the time-varying evolution caused by the receiver dynamics, where the order depends on the expected dynamics. In the following, the state-space formulation considering a 3rd order approximation is detailed, but the extension to a higher order is straightforward. The 3rd order Taylor expansion of the phase is given by

$$\theta_{d,k} = \theta_0 + 2\pi \left(f_{d,k} k T_s + \frac{1}{2} \dot{f}_{d,k} k^2 T_s^2 \right), \quad (13)$$

where θ_0 (rad) is a random constant phase value, $f_{d,k}$ (Hz) the carrier Doppler frequency shift and $\dot{f}_{d,k}$ (Hz/s) the Doppler frequency rate (*i.e.*, the Doppler dynamics). If the state to be tracked is $\mathbf{x}_k^* \doteq [\theta_{d,k} \ f_{d,k} \ \dot{f}_{d,k}]^T$, the process equation (phase expressed in cycles) is formulated as

$$\mathbf{x}_k^* = \underbrace{\begin{pmatrix} 1 & T_s & T_s^2/2 \\ 0 & 1 & T_s \\ 0 & 0 & 1 \end{pmatrix}}_{\text{transition matrix}} \mathbf{x}_{k-1}^* + \mathbf{v}_k, \quad (14)$$

where the transition matrix is denoted \mathbf{F}_d and the process noise, $\mathbf{v}_k \sim \mathcal{N}(0, \mathbf{P}_k)$, stands for possible uncertainties or mismatches on the dynamic model and the phase errors introduced by scintillation. The process noise covariance matrix \mathbf{P}_k is usually a priori designed (fixed value) according to the problem at hand and depending on the system working conditions. Equations (12) and (14) define the standard carrier tracking state-space formulation of the problem.

One of the key ideas of this contribution is to introduce the scintillation phase and amplitude into the state-space formulation. As shown in the previous section, the scintillation phase and amplitude are correctly modeled using an $AR(1)$ and $AR(2)$ model, respectively, which are mathematically written as

$$\theta_{s,k} = \beta_{1,1} \theta_{s,k-1} + \eta_{ph,k}, \quad (15)$$

$$\rho_{s,k} = c + \beta_{2,1} \rho_{s,k-1} + \beta_{2,2} \rho_{s,k-2} + \eta_{a,k}, \quad (16)$$

where $\beta_{1,1}$, $\beta_{2,1}$, $\beta_{2,2}$, $\sigma_{\eta_{ph}}^2$, $\sigma_{\eta_{\bullet}}^2$ and c are system model parameters, determined via simulation from the CSM time-series. From this approximated scintillation model, and taking into account that the state to be tracked is given by $\mathbf{x}_k = [\theta_{d,k} \ f_{d,k} \ \dot{f}_{d,k} \ \theta_{s,k} \ \rho_{s,k} \ \rho_{s,k-1}]^\top$, the process equation is

$$\mathbf{x}_k = \begin{pmatrix} \mathbf{F}_d & \mathbf{0}_3 \\ \mathbf{0}_3 & \mathbf{F}_s \end{pmatrix} \mathbf{x}_{k-1} + \mathbf{c} + \mathbf{w}_k, \quad (17)$$

where $\mathbf{c}^\top = [0 \ 0 \ 0 \ 0 \ c \ 0]$, $\mathbf{0}_3$ is the 3×3 null matrix, the scintillation transition matrix is defined as

$$\mathbf{F}_s = \begin{pmatrix} \beta_{1,1} & 0 & 0 \\ 0 & \beta_{2,1} & \beta_{2,2} \\ 0 & 1 & 0 \end{pmatrix}, \quad (18)$$

and the Gaussian noise vector is defined as $\mathbf{w}_k^\top = [\mathbf{v}_k^\top \ \eta_{ph,k} \ \eta_{a,k} \ 0]$, with diagonal covariance matrix $\mathbf{Q}_k = \text{diag}(\mathbf{P}_k, \sigma_{\eta_{ph}}^2, \sigma_{\eta_{\bullet}}^2, 0)$. Equations (12) and (17) define the new state-space formulation for scintillation mitigation.

4. ON STANDARD GNSS CARRIER TRACKING

The carrier phase tracking implemented during the last decades in standard communications receivers and mass-market satellite-based positioning systems rely on well-established PLL-based architectures [2, 28]. With the advent of software defined radio (SDR) receivers in real-life applications [29, 30], the KF-based schemes start to be taken into account as a strong alternative to traditional and advanced PLL-based solutions. In the following, the basics of both standard PLL and KF carrier tracking architectures are briefly summarized.

PLL-based Tracking Techniques

The standard PLL architecture is build up with three main blocks: a phase detector based on a discriminator, a filter and a carrier generator, which is driven by a numerically controlled oscillator (NCO). The phase detector produces an error signal which is proportional to the carrier phase error. The filter tries to minimize the difference between the carrier tracking stage input and a reference signal, that is, drives the carrier phase error to zero. The basic PLL architecture is sketched in Figure 6, together with a standard 2^{nd} order PLL loop filter and the NCO architecture, which is nothing but an integrator. In the absence of data bits, the optimal maximum likelihood (ML) estimator is the four quadrant arctangent discriminator, while the two quadrant arctangent discriminator is the preferred option when data is present in the signal. See [9] for a detailed discussion on the different discriminators and PLL architectures available in the literature.

As already pointed out in the introduction, the main problem of the standard PLLs is the existing noise reduction versus dynamic range tradeoff, which may lead the filter to lose lock, therefore somehow limiting the applicability of these architectures in challenging scenarios. This tradeoff is mainly driven by the bandwidth of the PLL: a small bandwidth is need to filter out the noise and a large bandwidth is mandatory to cope with fast phase variations. Notice that the PLL bandwidth is constant and a priori heuristically fixed by the user. The design and implementation simplicity of traditional PLLs turns to be the main drawback in time-varying scenarios.

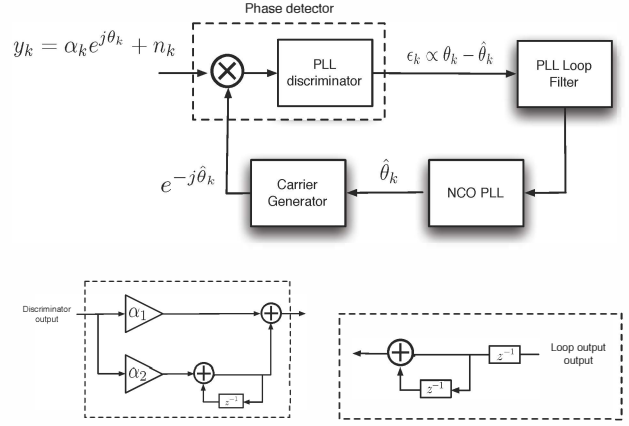


Figure 6. Basic PLL architecture (top), 2^{nd} order PLL loop filter (bottom - left) and NCO (bottom - right).

Still relying on the basic architecture, there are several ways to improve the stand-alone PLL performances, the most common in the literature being the FLL-assisted PLL (FPLL) [6] and the adaptive bandwidth PLL (APLL) [31]. The former uses a FLL permanently assisting a PLL, which reduces the apparent dynamics that the main PLL has to track, allowing the main loop to use a smaller bandwidth, thus filtering out more noise; while the latter uses a single PLL which automatically adjusts the loop bandwidth from the input working conditions. From an optimal filtering point of view, both PLL-based alternatives are suboptimal and still heuristically adjusted. The main reason why these techniques have been adopted in several applications is the implementation simplicity and tuning, but their performances have been clearly overcome by their KF-based counterpart.

KF-based Tracking Techniques

It is well known that for a time-invariant system with an a priori fixed Kalman gain, a 2^{nd} order PLL is equivalent to a 2^{nd} order KF in steady-state conditions [32]. In other words, for fixed working conditions where the Kalman gain has attained a constant steady-state value, there exists a PLL parametrization which is equivalent to the KF (i.e., the transient regime will be distinct because the PLL bandwidth is constant while the Kalman gain is time-dependant). From an architectural point of view, the general KF equations [33] can be particularized for the carrier tracking problem (e.g., the 2^{nd} order Kalman state is defined as $\mathbf{x}_k^\top = [\theta_k \ f_{d,k}]$ and interpreted to clearly see this equivalence. Comparing both architectures (i.e., the standard KF carrier tracking architecture is sketched in Figure 7), the innovations' sequence of the KF is the output of the discriminator, the estimated carrier phase is the output of the loop, and the predicted phase value is the input to the carrier generator. The natural question that arises from this resemblance is why the KF may perform better than the PLL if at the end they are equivalent? The answer relies on some important aspects listed hereafter:

- They are only equivalent in a very restrictive scenario, that is, in steady-state conditions, for time-invariant systems, and assuming that the PLL loop parameters have been optimally set according to the system working conditions (what may not be trivial).
- In general, the PLL loop filter parameters are set somehow heuristically and are constant during the full operation, while

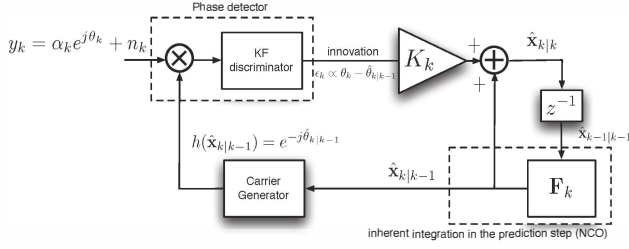


Figure 7. Standard KF-based carrier phase tracking architecture.

the Kalman gain is time-varying and optimally adjusted to the actual working conditions at every time-step. That is why the KF is always optimal (under the Gaussian assumption) and the PLL is always suboptimal.

- The previous consideration may have a strong impact in challenging and/or time-varying scenarios, because the PLL does not adapt to changing working conditions.

Using the state-space formulation given in (12) and (14), it is easy to construct a KF to solve the carrier phase tracking problem. Note that measurements y_k in (12) are not used directly in the filter implementation, but instead go through a discriminator to obtain the noisy phase measurements. This allows to use a traditional linear KF and avoids the derivation of suboptimal nonlinear solutions (*i.e.*, otherwise the measurement equation is nonlinear). Then, for the computation of the Kalman gain the measurement noise variance is needed. An expression for the approximated variance of the phase noise at the output of the ATAN discriminator is [34]

$$\sigma_{n_\theta}^2 = \frac{1}{8\pi^2 C/N_0 T_s} \left(1 + \frac{1}{2C/N_0 T_s} \right). \quad (19)$$

where C/N_0 stands for the carrier-to-noise density ratio. In this basic architecture the process covariance \mathbf{P}_k must also be specified according to the expected dynamics.

5. JOINT CARRIER TRACKING AND SCINTILLATION MITIGATION

In the previous section, the standard PLL and KF-based carrier tracking solutions have been introduced. The former is the well-established baseline receiver architecture, and the latter is the optimal and robust alternative, being a powerful option to be preferred in modern digital receivers to operate under non-nominal propagation conditions. But because of the estimation versus mitigation dilemma previously discussed, any of those two approaches provides a solid solution to the joint carrier tracking (*i.e.*, carrier dynamics due to the relative movement between the satellite and the receiver) and ionospheric scintillation mitigation problem.

In the sequel, an innovative solution to deal with this problem is detailed. Recall that the key idea is to model the scintillation phase and amplitude as an $AR(1)$ and an $AR(2)$ process, respectively. The measurement equation in (12) can be rewritten as

$$\begin{bmatrix} y_{i,k} \\ y_{q,k} \end{bmatrix} = A_k \rho_{s,k} \begin{bmatrix} \cos(\theta_k) \\ \sin(\theta_k) \end{bmatrix} + \begin{bmatrix} n_{i,k} \\ n_{q,k} \end{bmatrix}, \quad (20)$$

where $y_k = y_{i,k} + jy_{q,k}$, $n_k = n_{i,k} + jn_{q,k}$ and $\theta_k = \theta_{d,k} +$

Algorithm 1 Carrier phase tracking EKF formulation

Require: $\hat{\mathbf{x}}_0$, $\mathbf{P}_{x,0|0}$, \mathbf{Q}_k and $\sigma_{n,k}^2 \forall k$. $\mathbf{R}_k = \sigma_{n,k}^2/2 \times \mathbf{I}_2$.

- 1: Set $k \leftarrow 1$
- Time update (prediction)**
- 2: Estimate the predicted state:
 $\hat{\mathbf{x}}_{k|k-1} = \mathbf{F} \hat{\mathbf{x}}_{k-1|k-1}$.
- 3: Estimate the predicted error covariance:
 $\mathbf{P}_{x,k|k-1} = \mathbf{F} \mathbf{P}_{x,k-1|k-1} \mathbf{F}^\top + \mathbf{Q}_k$.
- Measurement update (estimation)**
- 4: Estimate the predicted measurement:
 $\hat{\mathbf{y}}_{k|k-1} = \mathbf{h}_k(\hat{\mathbf{x}}_{k|k-1})$.
- 5: Estimate the innovation covariance matrix:
 $\mathbf{P}_{y,k|k-1} = \mathbf{H}_k \mathbf{P}_{x,k|k-1} \mathbf{H}_k^\top + \mathbf{R}_k$.
Estimate the Kalman gain
 $\mathbf{K}_k = \mathbf{P}_{x,k|k-1} \mathbf{H}_k^\top \mathbf{P}_{y,k|k-1}^{-1}$.
- 6: Estimate the updated state
 $\hat{\mathbf{x}}_{k|k} = \hat{\mathbf{x}}_{k|k-1} + \mathbf{K}_k (\mathbf{y}_k - \hat{\mathbf{y}}_{k|k-1})$.
- 7: Estimate the corresponding error covariance:
 $\mathbf{P}_{x,k|k} = \mathbf{P}_{x,k|k-1} - \mathbf{K}_k \mathbf{H}_k \mathbf{P}_{x,k|k-1}$.
- 8: Set $k \leftarrow k + 1$ and go to step 2.

$\theta_{s,k}$, and the state evolution can be modeled by

$$\begin{bmatrix} \theta_{d,k} \\ f_{d,k} \\ \dot{f}_{d,k} \\ \theta_{s,k} \\ \rho_{s,k} \\ \rho_{s,k-1} \end{bmatrix} = \mathbf{F} \begin{bmatrix} \theta_{d,k-1} \\ f_{d,k-1} \\ \dot{f}_{d,k-1} \\ \theta_{s,k-1} \\ \rho_{s,k-1} \\ \rho_{s,k-2} \end{bmatrix} + \begin{bmatrix} 0 \\ 0 \\ 0 \\ 0 \\ c \\ 0 \end{bmatrix} + \begin{bmatrix} v_{1,k} \\ v_{2,k} \\ v_{3,k} \\ \eta_{ph,k} \\ \eta_{a,k} \\ 0 \end{bmatrix}, \quad (21)$$

where $\mathbf{v}_k = [v_{1,k} \ v_{2,k} \ v_{3,k}]^\top$ and

$$\mathbf{F} = \begin{pmatrix} 1 & T_s & T_s^2/2 & 0 & 0 & 0 \\ 0 & 1 & T_s & 0 & 0 & 0 \\ 0 & 0 & 1 & 0 & 0 & 0 \\ 0 & 0 & 0 & \beta_{1,1} & 0 & 0 \\ 0 & 0 & 0 & 0 & \beta_{2,1} & \beta_{2,2} \\ 0 & 0 & 0 & 0 & 1 & 0 \end{pmatrix}.$$

As already stated, this state-space formulation allows the filter to be aware of both scintillation phase and amplitude variations, being much more powerful than its standard version only taking into account the dynamics, $\theta_{d,k}$. As the measurement equation is nonlinear and the goal is to avoid to use discriminators as phase detectors, an EKF formulation is proposed, being the easiest way to cope with such nonlinearity. In the EKF formulation, instead of the measurement transition function $\mathbf{h}(\mathbf{x}_k)$, the linearized transition matrix (*i.e.*, $\mathbf{H}_k = \nabla \mathbf{h}_k(\mathbf{x}_k)|_{\mathbf{x}_k = \hat{\mathbf{x}}_{k|k-1}}$) in (22) is used, where $\hat{\theta}_{k|k-1} = \hat{\theta}_{d,k|k-1} + \hat{\theta}_{s,k|k-1}$.

The EKF formulation for this carrier phase tracking problem is sketched in Algorithm 1, where $\mathbf{y}_k = [y_{i,k} \ y_{q,k}]^\top$, and the discriminator free EKF-based carrier tracking architecture is shown in Figure 8. The standard KF notation is used for the estimated variables, that is, $k|k-1$ refers to the predicted estimate at time k using measurements up to time $k-1$, and $k|k$ refers to the estimated value at time k using measurements up to time k .

$$\mathbf{H}_k = \begin{bmatrix} -A_k \hat{\rho}_{s,k|k-1} \sin(\hat{\theta}_{k|k-1}) & 0 & 0 & -A_k \hat{\rho}_{s,k|k-1} \sin(\hat{\theta}_{k|k-1}) & A_k \cos(\hat{\theta}_{k|k-1}) & 0 & 0 \\ A_k \hat{\rho}_{s,k|k-1} \cos(\hat{\theta}_{k|k-1}) & 0 & 0 & A_k \hat{\rho}_{s,k|k-1} \cos(\hat{\theta}_{k|k-1}) & A_k \sin(\hat{\theta}_{k|k-1}) & 0 & 0 \end{bmatrix}. \quad (22)$$

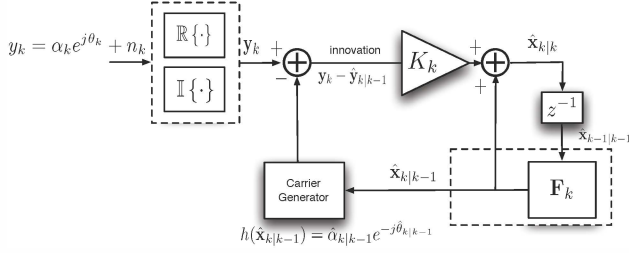


Figure 8. EKF-based carrier phase tracking architecture.

6. COMPUTER SIMULATIONS

In this section, in order to show the performance of the proposed approach, in contrast with what is being done in the literature (i.e., the current state-of-the-art methods include standard PLLs and KFs), illustrative numerical results are given for a carrier phase tracking example where the signal of interest is corrupted by severe scintillation. The simulated scenario considers that the filters are already in their steady-state regime, therefore the transient is not shown in the figures. From time $k = 0$ to 50 seconds the phase evolution includes only the variations due to dynamics (i.e., $\theta_k = \theta_{d,k}$), and then from $k = 50$ to 150 seconds on top of this dynamic behavior the signal is corrupted by severe ionospheric scintillation (i.e., $\theta_k = \theta_{d,k} + \theta_{s,k}$) with $S_4 = 0.8$ and $\tau_0 = 0.1$. The following parameters were used: simulation time $T_{sim} = 150$ s, integration time $T_s = 10$ ms, $C/N_0 = 35$ dB-Hz, an initial random phase in $[-\pi, \pi]$, $f_{d,0} = 5$ Hz (Doppler) and $\dot{f}_{d,0} = 0.1$ Hz/s (Doppler rate). To obtain statistically significant results, the root mean square error (RMSE) was used as a measure of performance, and obtained from 200 Monte Carlo runs.

For the sake of completeness four methods were considered:

- 3rd order PLL with bandwidth $B_{PLL} = 10$ Hz.
- Standard KF tracking the phase, Doppler and Doppler rate.
- Augmented state standard KF (using a discriminator type architecture) considering only an $AR(1)$ approximation for the scintillation phase, named hereafter KF-AR, as introduced in [19].
- New extended KF tracking phase dynamics together with scintillation phase and amplitude, named EKF-AR.

First of all, the scintillation amplitude and phase estimates given by the EKF-AR filter are shown in Figure 9 for a single realization. Notice that the filter is able to correctly track the scintillation amplitude, and to completely decouple the phase contribution due to scintillation from the one due to the relative movement between the satellite and the receiver. These results show that for a correctly adjusted $AR(1)$ model for the scintillation phase and $AR(2)$ model for the scintillation amplitude evolution, the proposed filter may be a very powerful scintillation mitigation solution.

The RMSE obtained with the different methods is shown in Figure 10. The results show the very good performance and correct scintillation mitigation given by the EKF-AR with respect to the other methods. It is clear that the worst perfor-

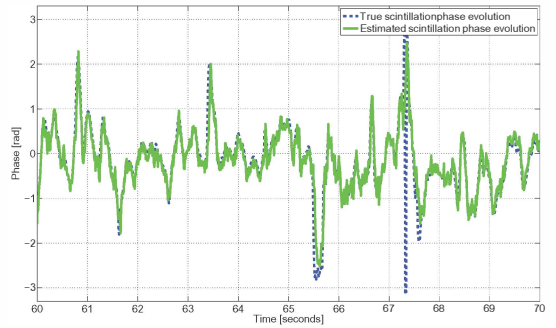
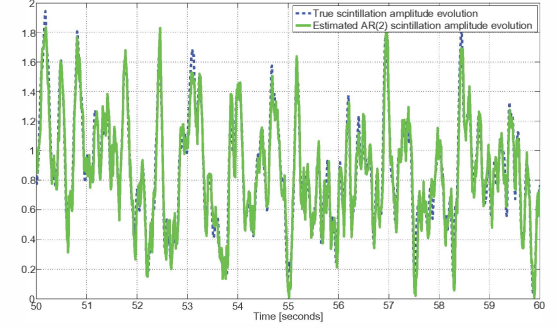


Figure 9. Example of the scintillation amplitude (top) and phase (bottom) estimates for a single realization of the filter.

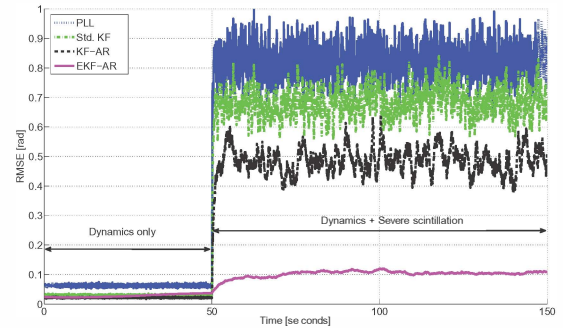


Figure 10. Comparison of the RMSE obtained with the four different methods: 3rd order PLL, standard KF, standard KF-AR and the new EKF-AR.

mances are obtained with the constant bandwidth traditional PLL approach. Then, even if the standard KF overcome some of the limitations of the PLLs in standard scenarios, is not able to correctly cope with the scintillation in this case. The EKF-AR also clearly outperforms the KF-AR, which only includes the $AR(1)$ approximation of the scintillation phase into the state and considers a traditional discriminator-based architecture. Therefore, from these results one can conclude that the proposed EKF-AR is the best option for scintillation mitigation.

7. CONCLUSIONS

This paper presented a new KF-based approach to deal with robust carrier phase tracking under ionospheric scintillation conditions, and in particular to cope with the challenging scintillation mitigation problem in modern GNSS receivers. In the proposed methodology, both scintillation phase and amplitude fluctuations are modeled using an autoregressive (AR) process and then embedded into the carrier tracking state-space formulation. Including the scintillation complex gain into the filter formulation has been proven to be a very good way to cope with such undesired effect. From the different alternatives available in the literature the proposed approach is the only one capable to decouple the scintillation phase contribution from the Doppler carrier phase dynamics, providing a promising and powerful framework to cope with the estimation versus mitigation dilemma. The EKF-based solution has been tested in a simulated scenario, where a GNSS signal was corrupted by severe scintillation, and compared to current state-of-the-art methods clearly showing the improved performance. Future work goes towards the recursive detection and estimation of the scintillation parameters, to obtain a fully adaptive scintillation mitigation solution.

REFERENCES

- [1] U. Mengali and A. N. D'Andrea, *Synchronization Techniques for Digital Receivers*, Plenum Press, New York, USA, 1997.
- [2] E. D. Kaplan, Ed., *Understanding GPS: principles and applications*, Artech House, 2nd edition, 2006.
- [3] P. M. Kintner, T. E. Humphreys, and J. Hinks, "GNSS and ionospheric scintillation. How to survive the next solar maximum," *Inside GNSS*, pp. 22–33, July/Aug. 2009.
- [4] P. Lian, *Improving tracking performance of PLL in high dynamic applications*, Ph.D. thesis, University of Calgary, Calgary, Canada, 2004.
- [5] L. Zhang and Y. T. Morton, "Tracking GPS signals under ionosphere scintillation conditions," in *Proc. of the ION GNSS*, Sept. 2009, pp. 227–234.
- [6] X. Mao, Y. T. Morton, L. Zhang, and Y. Kou, "GPS carrier signal parameters estimation under ionosphere scintillation," in *Proc. of the ITM - ION*, Portland, OR, Sept. 21–24, 2010.
- [7] G. Skone, G. Lachapelle, D. Yao, W. Yu, and R. Watson, "Investigating the impact of ionospheric scintillation using a GPS software receiver," in *Proc. of the ION GNSS*, Long Beach, CA, Sept. 13–16, 2005.
- [8] W.-L. Mao and A.-B. Chen, "Mobile GPS carrier phase tracking using a novel intelligent dual-loop receiver," *Intl. Journal of Satellite Communications and Networking*, vol. 26, pp. 119–139, 2008.
- [9] J. López-Salcedo, J. Peral-Rosado, and G. Seco-Granados, "Survey on robust carrier tracking techniques," *IEEE Commun. Surveys & Tutorials*, vol. 16, no. 2, pp. 670–688, April 2014.
- [10] R. Sarnadas, T. Ferreira, J. Vilà-Valls, G. Seco-Granados, J. López-Salcedo, F. D. Nunes, F. M. G. Sousa, P. Crosta, F. Zanier, and R. Prieto-Cerdeira, "Trade-off analysis of robust carrier phase tracking techniques in challenging environments," in *Proc. of the ION GNSS+*, Sept. 2013.
- [11] J.-H. Won, T. Pany, and B. Eissfeller, "Characteristics of Kalman filters for GNSS tracking loops," *IEEE Trans. on Aerospace and Electronic Systems*, vol. 48, no. 4, pp. 3671–3681, Oct. 2012.
- [12] T. E. Humphreys et al., "GPS carrier tracking loop performance in the presence of ionospheric scintillations," in *Proc. of the ION GNSS*, 2005.
- [13] W. Yu, G. Lachapelle, and S. Skone, "PLL performance for signals in the presence of thermal noise, phase noise, and ionospheric scintillation," in *Proc. of the ION GNSS*, Fort Worth, TX, Sept. 2006.
- [14] C. W. Hu et al., "Adaptive Kalman filtering for vehicle navigation," *Journal of Global Positioning Systems*, vol. 2, no. 1, pp. 42–47, 2003.
- [15] L. Zhang, Y. T. Morton, and M. M. Miller, "A variable gain adaptive Kalman filter-based GPS carrier tracking algorithms for ionosphere scintillation signals," in *Proc. of the ITM - ION*, 2010, pp. 3107–3114.
- [16] K.-H. Kim, G.-I. Jee, and J.-H. Song, "Carrier tracking loop using the adaptive two-stage kalman filter for high dynamic situations," *Intl. Journal of Control, Automation and Systems*, vol. 6, no. 6, pp. 948–953, 2008.
- [17] J.-H. Won, B. Eissfeller, T. Pany, and J. Winkel, "Advanced signal processing scheme for GNSS receivers under ionospheric scintillation," in *Proc. of the IEEE/ION PLANS*, 2012, pp. 44–49.
- [18] J. Vilà-Valls, P. Closas, and C. Fernández-Prades, "On the identifiability of noise statistics and adaptive KF design for robust GNSS carrier tracking," in *Submitted to the IEEE Aerospace Conference*, March 2015.
- [19] J. Vilà-Valls, J. López-Salcedo, and G. Seco-Granados, "An interactive multiple model approach for robust gnss carrier phase tracking under scintillation conditions," in *Proc. IEEE International Conference on Acoustics, Speech and Signal Processing (ICASSP)*, May 2013.
- [20] T. Ferreira, R. Sarnadas, J. Vilà-Valls, J. López-Salcedo, G. Seco-Granados, P. Crosta, R. Prieto-Cerdeira, and F. Zanier, "Characterization of carrier phase tracking techniques under ionosphere scintillation scenarios," in *Proc. 6th European Workshop on GNSS Signals and Signal Processing*, Dec. 2013.
- [21] T. E. Humphreys et al., "Simulating ionosphere-induced scintillation for testing GPS receiver phase tracking loops," *IEEE Journal of Selected Topics in Signal Processing*, vol. 3, no. 4, pp. 707–715, Aug. 2009.
- [22] T. E. Humphreys, M. L. Psiaki, and P. M. Kintner, "Modeling the effects of ionospheric scintillation on GPS carrier phase tracking," *IEEE Trans. on Aerospace and Electronic Systems*, vol. 46, no. 4, pp. 1624–1637, Oct. 2010.
- [23] International Telecommunication Union (ITU), "Ionospheric propagation data and prediction methods required for the design of satellite services and systems. recommendation itu-r p.531-12," Tech. Rep., Sept. 2013.
- [24] G. Di Giovanni and S. M. Radicella, "An analytical model of the electron density profile in the ionosphere," *Advances in Space Research*, vol. 10, no. 11, pp. 27–30, Nov. 1990.
- [25] T. E. Humphreys et al., "A data-driven testbed for evaluating GPS carrier tracking loops in ionospheric scintillation," *IEEE Trans. on Aerospace and Electronic Systems*, vol. 46, no. 4, pp. 1609–1623, Oct. 2010.

- [26] S. M. Kay, *Fundamentals of Statistical Signal Processing: Estimation Theory*, Prentice-Hall, Englewood Cliffs, New Jersey, USA, 1993.
- [27] J. J. Spilker, "Fundamentals of signal tracking theory," in *Global Positioning System: Theory and Applications*, Vol. 1, B. W. Parkinson and J. J. Spilker, Eds., pp. 245–328. American Institute of Aeronautics and Astronautics, 1996.
- [28] H. Meyr, M. Moeneclaey, and S. Fetchel, *Digital Communication Receivers: Synchronization, Channel Estimation and Signal Processing*, Wiley Series in Telecommunications and Signal Processing, New York, USA, 1998.
- [29] C. Fernández-Prades, J. Arribas, P. Closas, C. Avilés, and L. Esteve, "GNSS-SDR: An open source tool for researchers and developers," in *Proc. of the ION GNSS 2011 Conference*, Portland, Oregon, Sept. 2011.
- [30] Ifen, GmbH, "SX-NSR GNSS Receiver," Datasheet, May 2013.
- [31] F. Legrand, *Spread spectrum signal tracking loop models and raw measurements accuracy improvement method*, Ph.D. thesis, INP Toulouse, Toulouse, France, 2002.
- [32] A. Patapoutian, "On phase-locked loops and Kalman filters," *IEEE Trans. on Communications*, vol. 47, no. 5, pp. 670–672, May 1999.
- [33] B. Anderson and J. B. Moore, *Optimal filtering*, Prentice-Hall, Englewood Cliffs, New Jersey, USA, 1979.
- [34] C. Gernot, *Development of Combined GPS L1/L2C Acquisition and Tracking Methods for Weak Signals Environments*, Ph.D. thesis, Department of Geomatics Engineering, University of Calgary, Canada, 2009.

BIOGRAPHY



Pau Closas received the M.Sc. and Ph.D. in Electrical Engineering from the Universitat Politècnica de Catalunya (UPC) in 2003 and 2009, respectively. He holds a M.Sc. degree in Advanced Mathematics and Mathematical Engineering from UPC since 2014. In 2003, he joined the Department of Signal Theory and Communications, UPC, as a Research Assistant. During 2008 he was Research Visitor at the Stony Brook University (SBU), New York, USA. In 2009 he joined the CTTC, where he currently holds a Senior Researcher position and is the Head of the Statistical Inference for Communications and Positioning Department in the Communications Systems Division. His primary areas of interest include statistical and array signal processing, estimation and detection theory, Bayesian filtering, robustness analysis, and game theory, with applications to positioning systems, wireless communications and mathematical biology. Pau Closas is the recipient of the EURASIP Best PhD Thesis Award 2014 and the 9th Duran Farell Award for Technological Research from UPC for sustained research in advanced GNSS receiver design.



Carles Fernández-Prades received the M.Sc. and Ph.D. (cum-laude) degrees in Electrical Engineering from the Universitat Politècnica de Catalunya (UPC) in 2001 and 2006, respectively. In 2001, he joined the Department of Signal Theory and Communication at UPC as a Research Assistant, getting involved in European and National research projects both with technical and managerial duties. He also was Teaching Assistant in the field of Analog and Digital Communications (UPC 2001-2005). In 2006 he joined CTTC, where he currently holds a position as Senior Researcher and serves as Head of the Communications Systems Division. His primary areas of interest include signal processing, estimation theory and nonlinear Bayesian filtering, with applications in positioning, communications systems, software radio and the design of RF front-ends.



Jordi Vilà-Valls received the Ph.D. degree in Electrical Engineering from the Grenoble Institute of Technology (INPG), Grenoble, France, in 2010. He was a Postdoctoral Research Associate with the Signal Processing and Communications (SPCOM) group, UPC (2010-12); and with the Signal Processing for Communications and Navigation (SPCOMNAV) group, UAB (2012-13).

In 2014 he joined the CTTC as a Research Associate at the Statistical Inference Department. His primary areas of interest include statistical signal processing, estimation and detection theory, nonlinear Bayesian estimation, robustness and adaptive methods; with applications to positioning, localization and tracking systems, communications, aerospace and seismology.